ACS APPLIED MATERIALS & INTERFACES

Research Article

www.acsami.org

Cosynthesis of Cargo-Loaded Hydroxyapatite/Alginate Core–Shell Nanoparticles (HAP@Alg) as pH-Responsive Nanovehicles by a Pre-gel Method

Yung-He Liang,[†] Chia-Hung Liu,[‡] Shih-Hsiang Liao,[†] Yuan-Yun Lin,[†] Hao-Wei Tang,[†] Shin-Yun Liu,[§] I-Rue Lai,[§] and Kevin C.-W. Wu*[,†,⊥]

[†]Department of Chemical Engineering, National Taiwan University, No. 1, Sec. 4, Roosevelt Road, Taipei 10617, Taiwan

[‡]Department of Urology, Taipei Medical University-Shuang Ho Hospital, No. 291, Jhongjheng Road, Jhonghe District, New Taipei City 23561, Taiwan

[§]Graduate Institute of Anatomy and Cell Biology, College of Medicine, National Taiwan University, Taipei 10764, Taiwan

[⊥]Division of Medical Engineering Research, National Health Research Institutes, 35 Keyan Road, Zhunan, Miaoli County 350, Taiwan

Supporting Information

ABSTRACT: A new core–shell nanostructure consisting of inorganic hydroxyapatite (HAP) nanoparticles as the core and organic alginate as the shell (denoted as HAP@Alg) was successfully synthesized by a pre-gel method and applied to pH-responsive drug delivery systems (DDS). HAP@Alg nanoparticles have the advantages of hydroxyapatite and alginate, where hydroxyapatite provides pH-responsive degradability, and alginate provides excellent biocompatibility and COOH functionality. Through the subsequent addition of $CaCl_2$ and phosphate solutions to the alginate solution, HAP@Alg nanoparticles with controllable particle sizes (ranging from 160 to 650 nm) were obtained, and their core–shell structure was confirmed through transmission electron microscopy (TEM) observation. Rhodamine 6G (R6G), a positively charged dye, was selected as a model drug for pH-sensitive DDS. R6G was encapsulated in the HAP/Alg nanoparticles upon synthesis, and its loading efficiency could reach up to approximately 63.0%. The in vitro release behavior of the loaded R6G at different pH values was systematically studied, and the results indicated that more R6G molecules were released at lower pH conditions. For example, after releasing for 8 h, the release amount of R6G at pH 2.0 was 2.53-fold the amount at pH 7.4. We attributed this pH-sensitive release behavior to the dissolution of the HAP core in acidic conditions. The results of the MTT assay and confocal laser scanning microscopy indicated that the HAP@Alg were successfully uptaken by liver cancer cells (HepG2) without apparent cytotoxicity. The synthesized HAP@Alg nanoparticles show great potential as drug nanovehicles with high biocompatibility, enhanced drug loading, and pH-responsive features for future intracellular DDS.

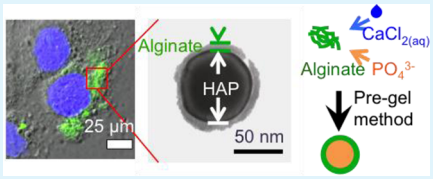

KEYWORDS: *hydroxyapatite, alginate, nanoparticles, pH-responsive release, DDS, HepG2*

1. INTRODUCTION

The direct administration of conventional anticancer drugs results in limited efficacy and exerts serious adverse side effects on the patient. A drug delivery system, in general, can refer to any one of numerous strategies to overcome these problems.[1−3] Particles with nanometric sizes have proven useful for loading therapeutic drugs, protecting them from enzymatic degradation, alternating their release profiles, and transporting them to target sites.[4−6] An ideal nanocarrier should be biocompatible and allow a high loading capacity for the drug.

Alginate, a natural polysaccharide, is recognized as the most abundant marine biopolymer in the world, and it is known for its high biocompatibility and biodegradability.[7−9] For decades, alginate has been used as a thickener, an emulsifier, and a stabilizer in the food industry because it is generally regarded as safe (GRAS) by the U.S. Food and Drug Administration (GRN No. 328). Alginate is composed of the epimers D-mannuronic acid (M) and L-guluronic acid (G) residues, and these monomers are (1→4) linked and arranged in homogeneous blocks (MM, GG), as well as heterogeneous blocks (MG). When multiple G-blocks are aligned side by side, they form a three-dimensional network, thereby producing a junction that is suitable for cooperative binding with divalent and multivalent cations (except Mg^{2+}). The conformation of guluronic acid allows a high degree of coordination of the COO^- and OH^- groups with Ca^{2+}. This characteristic structure is often called an "egg-box" model.[9] After the reaction with Ca^{2+}, alginate forms a high-viscosity gel. In contrast to conventional drug loading processes wherein drugs are adsorbed onto the pre-synthesized carriers, the unique cation-induced gelation properties of alginate enable the encapsulation of therapeutic agents with an enhanced loading. In terms of drug delivery, microparticles

Received: September 5, 2012
Accepted: November 15, 2012
Published: November 15, 2012

   dx.doi.org/10.1021/am301895u | ACS Appl. Mater. Interfaces 2012, 4, 6720–6727

Scheme 1. Illustration for Cosynthesis of Drug-Loaded Hydroxyapatite/Alginate Core-Shell Nanoparticles; Drugs Can Be In situ Loaded into the Nanoparticles through (a) Route 1 and (b) Route 2

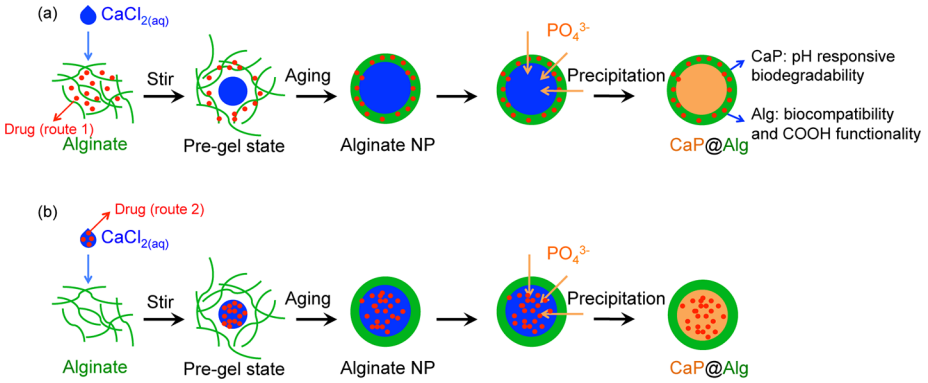

Table 1. Summary of the Effects of Various Synthetic Conditions on the Particle Sizes and Zeta-Potentials; Particles were Collected by Dialysis or Centrifugation

synthetic conditions	separation	Ca (mmol)	P/Ca (mol/mol)	size (nm)	PDI	zeta-potential (mV)
1-1	dialysis	0.1	1.00	760.6	0.747	−69.9
1-2		0.1	2.25	527.6	0.899	−61.8
1-3		0.1	4.50	497.9	0.364	−71.0
1-4		0.1	7.50	1027	0.543	−76.7
1-5		0.2	1.00	1226	0.672	−49.4
1-6		0.2	2.25	654.2	0.427	−34.6
1-7		0.2	4.50	482.1	0.302	−77.6
1-8		0.2	7.50	1053	0.658	−56.3
2-1	centrifugation	0.1	1.00	590.0	0.554	−27.3
2-2		0.1	2.25	232.5	0.369	−22.1
2-3		0.1	4.50	190.3	0.132	−28.8
2-4		0.1	7.50	227.3	0.211	−54.3
2-5		0.2	1.00	254.3	0.210	−27.3
2-6		0.2	2.25	160.3	0.184	−27.8
2-7		0.2	4.50	173.9	0.153	−38.4
2-8		0.2	7.50	223.3	0.151	−59.2

or microcapsules made of alginate have been used successfully,[10−12] but the fabrication of alginate nanoparticles is relatively limited because of the persistence of alginate, which makes the polymer chain stiff and hard to operate on a nanometric scale.

Drug carriers have been administrated widely by intravenous injection, which guarantees the highest bioavailability (100% by definition).[13] In such cases, particle size is the most important factor in terms of biodistribution and cellular uptake.[14] Sizes of approximately 100 nm are preferred because particles of this size are hardly recognized by the immune system. Furthermore, they show a high colloidal stability and long circulating half-life time. Therefore, they are more likely to accumulate in tumor tissues through the enhanced permeability and retention (EPR) effect.[15,16] In addition, particles with pH responsibility are useful for controlled release inside cancer cells, because cellular endosome is an acidic environment with a pH of approximately 4.5.[17−19] Therefore, the development of alginate-based nanoparticles with pH-sensitivity and a particle size of approximately 100 nm is highly desired.

Rajaonarivony et al. reported the first poly-L-lysine/alginate nanoparticles by using a pre-gel method.[20] The term "pre-gel" refers to a stage in the crosslinking process that extends up to, but not beyond, the gel point.[21] By controlling the amount of calcium and the rate of calcium addition, a pre-gel state of alginate (i.e., a microdomain with a high concentration of alginate) can be obtained.[9] De et al. reported a similar chitosan/alginate system produced by a modified pre-gel method using positively charged chitosan.[22] Yu et al. reported a modified pre-gel method used to synthesize $CaCO_3$/alginate nanoparticles by sequent additions of calcium cations and phosphate anions. In addition, a low-molecular-weight anticancer drug, 5-fluorouracil (5-FU), was loaded in the synthesized $CaCO_3$/alginate nanoparticles for the DDS.[23]

In this study, we adopted the concept of the pre-gel method to synthesize a new core-shell nanoparticle consisting of an inorganic hydroxyapatite as the core and an organic alginate biopolymer as the shell (Scheme 1). This method was used for several reasons: (1) alginate provides excellent biocompatibility and surface functionality (COOH group), (2) hydroxyapatite also exhibits high biocompatibility and, more significantly, pH-responsible biodegradability, and (3) drugs can be loaded and core−shell nanostructures can be synthesized simultaneously, thereby enhancing the drug packing capability. We then characterized the synthesized HAP@Alg nanoparticles with X-ray diffraction (XRD), transmission electron microscopy (TEM), Fourier transform infrared spectroscopy (FTIR), and thermo-gravimetric analysis (TGA). In addition, a model drug, rhodamine 6G (R6G), and an anticancer drug, doxorubicin (DOX), were encapsulated during the synthesis process with enhanced efficiency. The R6G-loaded HAP@Alg nanoparticles showed pH-dependent in vitro release behaviors, and for

intracellular drug delivery, the DOX-loaded HAP@Alg nanoparticles increased the drug's cell-killing efficiency, compared to free drugs.

2. MATERIALS AND METHODS

2.1. Chemicals. Alginate (cat# A2158), sodium phosphate dibasic (Na_2HPO_4), calcium chloride dihydrate ($CaCl_2 \cdot 2H_2O$), rhodamine 6G (R6G), sodium acetate, acetic acid, dimethyl sulfoxide (DMSO), 4′,6-diamidino-2-phenylindole dihydrochloride (DAPI), phosphate buffered saline (PBS), and thiazolyl blue tetrazolium bromide (MTT) were purchased from Sigma-Aldrich. 5(6)-Carboxyfluorescein (CF) was provided by Acros. MEM Eagle, RPMI, fetal bovine serum (FBS), sodium bicarbonate (7.5 wt %), L-glutamine (200 mM in saline), and Pen-Strep Sol. (penicillin 10 000 units/mL and streptomycin 10 mg/mL) were provided by Biological Industries.

2.2. Synthesis of HAP@Alg-Based Nanoparticles. For the synthesis of HAP@Alg nanoparticles without cargo, alginate (0.1 g) was dissolved in DI water (25 mL) by stirring in a pre-equilibrated oil bath (55 °C) for 30 min. To this system was added a solution containing $CaCl_2$ (0.02M or 0.04M, 5 mL) at a rate of 30 mL/h. After 1 h, an Na_2HPO_4 solution (3 mL) was added at the same rate. The mixture was stirred for an additional 20 h, and then cooled to room temperature in a water bath. The solids were collected by either dialysis or centrifugation/re-dispersion. For dialysis, samples were transferred to a dialysis bag (Cellu•Sep T4; Nominal MWCO: 12 000−14 000, Orange Scientific, Belgium) and dialyzed against 500 mL DI water for 1 day. The DI water was refreshed every 8 h. For centrifugation, samples were placed in a centrifuge (Mikro 120; Hettich ZENTRIFUGEN) at 13 000 rpm for 30 min to remove the supernatant and washed with DI water 3 times to collect the pellets. The detailed synthetic conditions are shown in Table 1.

For the synthesis of HAP@Alg nanoparticles loaded with cargo molecules (i.e., R6G or CF), the synthetic condition 2-7 was used (i.e., $CaCl_2$ (0.04M, 5 mL), Na_2HPO_4 (0.3M, 3 mL), and centrifugation). During the synthesis, the R6G and CF molecules (1 mg) were first dissolved in the $CaCl_2$ solution and then added to the alginate solution.

2.3. Characterization. The hydrodynamic particle size and zeta potential of the synthesized HAP@Alg nanoparticles were measured by the Zetasizer Nano ZS system (Malvern Instruments Ltd., UK) at 25 °C with DI H_2O as the solvent. Samples were sonicated for 1 h before measuring. The average particle size was evaluated on the basis of dynamic light scattering (DLS). The morphology and core−shell structure of the samples were observed using an SEM (Nova Nano SEM) and a TEM (JEOL JEM-1200EX II). Sample-containing solutions were sonicated for 1 h, dropped onto copper grids (200 mesh, carbon-coated) and dried under vacuum. Before SEM observation, the samples were subjected to Pt coating. Spectra obtained from Fourier transform infrared spectroscopy (FTIR) were measured on a Perkin Elmer Spectrum 100 at a resolution of 4 cm^{-1}. Samples used for FTIR measurements were prepared by mixing the vacuum-dried samples with KBr (KBr : sample = 100:1). The mixture was then ground extensively and pressed into a translucent disc. The structural properties of the samples were analyzed by X-ray diffraction (XRD) on a Rigaku ultima IV system with Cu Kα radiation (λ = 1.5418 Å, 40 kV, 40 mA). The proportions of P and Ca were analyzed by inductively coupled plasma mass spectrometry (ICP-MS, Agilent 7500ce). Thermogravimetric analysis (TGA) curves were recorded on a Perkin Elmer PYRIS 1 DSC. Samples (5 mg) were maintained at 50 °C for 10 min, then heated to 800 °C at 10 °C/min and maintained at 800 °C for 1 min. Nitrogen flow was fixed at 20.0 mL/min throughout the measurement process.

2.4. Drug Loading and In vitro Release. For the loading of R6G molecules, the R6G-loaded samples were separated from the solution by centrifugation, and the supernatant was collected. The fluorescence of the supernatant was measured by PL (Hitachi F-7000 Fluorescence Spectrophotometer) to quantify the amount of R6G in the supernatant (λ_{ex}, 526 nm; λ_{em}, 551 nm). The loading efficiency and capacity were calculated according to the following equations.[23]

$$\text{encapsulation efficiency}(\%) = \frac{\text{drug input (mg)} - \text{drug in supernatant (mg)}}{\text{drug input (mg)}} \times 100\%$$

$$\text{loading capacity (mg/g)} = \frac{\text{drug input (mg)} - \text{drug in supernatant (mg)}}{\text{drug} - \text{loaded material (g)}}$$

For the in vitro release of R6G molecules, the R6G-loaded particles recovered by centrifugation (2.8 mg) were mixed with 10 mM acetate buffer at varying pH values (1.6 mL) at 37 °C. At predetermined time intervals, the mixture was centrifuged (13000 rpm, 30 min), and 0.4 mL of the supernatant was extracted and replaced with fresh buffers. R6G in the supernatant was quantified by measuring its fluorescence.

2.5. Cell Culture and MTT Assay. BT-20 human breast-cancer cells (ATCC no. HTB-19TM) and HepG2 cells were purchased from the National Health Research Institutes (NHRI), Taiwan. BT-20 cells were incubated in flasks with MEM medium at 37 °C, 5% CO_2, and 95% humidified atmosphere and were sub-cultured every 3 days. Each 100 mL of MEM was supplemented with 10 mL of FBS, 2 mL of $NaHCO_3$, 1 mL of L-glutamine, and 1 mL of Pen-Strep Sol. (penicillin 10 000 units/mL and streptomycin 10 mg/mL). HepG2 cells were incubated in flasks with RPMI medium at 37 °C, 5% CO_2, and 95% humidified atmosphere and were sub-cultured every 3 days. Each 100 mL of RPMI was supplemented with 10 mL of FBS and 1 mL of Pen-Strep Sol. (penicillin 10 000 units/mL and streptomycin 10 mg/mL). Cell viability was measure by MTT assay. BT-20 and HepG2 cells were seeded onto 24-well plates at a density of 1×10^5 cells/well and allowed to attach overnight. The medium was then removed and each well was washed twice with 1 mL PBS. Media containing samples with various concentrations were added to each well, and the cells were incubated at 37 °C for 24 h. The medium was then removed, and the wells were washed twice with 1 mL PBS. To each well 0.5 mL of MTT solution (0.5 mg/mL in the medium) was added, and the cells were incubated for an additional 4 h. The medium was then replaced with 0.5 mL DMSO. The plates were left stationary for 4 h to dissolve the blue crystals, and the absorbance was recorded by a microplate reader at a wavelength of 570 nm. Cell viability was expressed as the average absorbance of treated samples, relative to untreated ones.

2.6. Confocal Laser Scanning Microscopy (CLSM). HepG2 cells were seeded onto 4-well Lab-Tek slides at a density of 2.5×10^4 cells per well. After incubation at 37 °C with 5% CO_2 overnight, the medium was removed, and the slides were washed twice with PBS. To each well 0.5 mL PBS (10% FBS) containing CF-loaded HAP@Alg (100 μg/mL) was added. After incubation for an additional 2 h, the supernatant was removed, and the slides were washed extensively with PBS. To each well was added 0.5 mL of PBS containing 28 μM DAPI to stain the nuclei for 20 min. The slides were then washed 3 times with PBS and covered with coverslips. CLSM was performed on a Leica TCS SP5 II equipped with a 63x oil immersion objective lens. Blue fluorescence was produced in the DAPI-stained nuclei by exciting the cells with a UV laser (λ_{ex}: 405 nm). The green fluorescence emitted from the CF-loaded HAP@Alg was visualized by excitation at 488 nm.

3. RESULTS AND DISCUSSION

3.1. Synthesis and Characterization of HAP@Alg Nanoparticles. As shown in Scheme 1, a $CaCl_2$ solution with a desired concentration was added slowly to an alginate solution to induce the pre-gel state of alginate. The amount of Ca^{2+} solution has a significant effect on the gelation of alginate. An excessive amount of Ca^{2+} ions caused aggregation, and the maximum amount of Ca^{2+} for obtaining a homogeneous solution was 20 mmol (0.04M, 5 mL). Because alginate consists of D-mannuronic acid (M) and L-guluronic acid (G) with highly negative charges that can interact strongly with divalent cations

such as Ca^{2+}, the pre-gel state of alginate represents the egg-box structure of alginate−Ca^{2+},[9] resulting in the formation of nanoparticles.

The addition of phosphate ions was essential for stabilizing the nanoparticles. Without phosphate ions, the products were highly unstable for the DLS and TEM measurements. When phosphate ions were added to the mixture, they interacted with Ca^{2+}, thereby resulting in the formation of calcium phosphate nanoparticles. The nanoparticles were collected by either dialysis or centrifugation. The particle sizes of the samples synthesized at varying reaction conditions were analyzed by DLS, and they are summarized in Table 1. The samples collected by dialysis (samples 1-1 to 1-8) exhibited larger particle sizes (480−1200 nm) than those (samples 2-1 to 2-8) collected by centrifuge (160−250 nm, except for sample 2-1) under the same synthetic conditions. Furthermore, the dialysis-collected samples showed a higher negative surface charge than that of the centrifuge-collected samples. These results indicate that more negatively charged phosphate anions and alginate molecules were located on the external surface of the dialysis-collected samples. We suggest that this was because centrifuge would only cause precipitation of matters with "higher density", matters with "lighter density" such as free phosphate ions and alginate oligomers would stay in the supernatant and would not be collected with HAP@Alg NPs, resulting in less negatively charged surface.

The P/Ca molar ratio also affected the final particle size. We found that the minimum particle size could be obtained when the P/Ca value was 4.5, regardless of the type of collection method (i.e., samples 1-7 and 2-7). We analyzed the real P/Ca molar ratio of sample 2-7 by ICP-MS, and the result of 0.64 was significantly close to the ratio of conventional hydroxyapatite (i.e., P/Ca = 0.6). This result suggests that a consolidated HAP core can be formed under this condition. Further evidence was supported by the lowest poly-dispersity indices (PDI) of sample 2-7, among other samples. Therefore, we propose that phosphate ions play a role in strengthening the structure of the HAP@Alg nanoparticles. If phosphate ions were too few, it would be difficult to form HAP cores in the nanoparticles, and thus the synthesized nanoparticles would consist mainly of organic alginate polymers that were loose and unstable despite their large sizes. Furthermore, previous studies have found that the dissolution/erosion of calcium-alginate can be accelerated by the presence of a chelating reagent, such as phosphate or citrate, in the system.[24] An excessive amount of phosphate ions would disturb the coordination between alginate and calcium, thereby resulting in larger particle sizes. The effect of phosphate is therefore delicate, and the amount of phosphate must be chosen carefully. We use sample 2-7 for further characterization hereafter unless extra declaration.

The morphology and the core-shell structure of Sample 2-7 were observed by SEM and TEM, respectively. As shown in Figure 1a, a particle exhibiting a nearly spherical shape and a size of approximately 100 nm in diameter was observed. This particle size is significantly smaller than the one measured by DLS, because alginate interacts strongly with water and increases significantly in volume when placed in aqueous environments. Even with the shrinkage of the HAP@Alg nanoparticles after sample 2-7 was dried for observation under TEM, a clear difference between the inorganic HAP core and organic alginate polymer shell could be observed in the TEM image (Figure 1b). Although the shell was thin (approximately 10 nm) compared to the inorganic core (80 nm), it could be

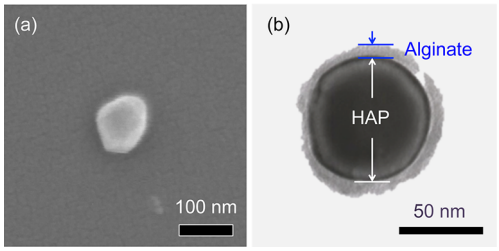

Figure 1. (a) SEM and (b) TEM images for typical HAP@Alg nanoparticles synthesized at the synthetic condition 2−7.

expected to swell when the sample is dispersed in an aqueous solution because of the bibulous property of alginate. We therefore propose that the alginate shell can act as a barrier to control molecule diffusion, whereas the inner HAP core can serve as a pH-sensitive element.

To investigate the crystalline phase of the inner calcium phosphate, we examined sample 2-7 by XRD and ICP-MS. In contrast to the XRD pattern of pure amorphous alginate exhibiting no peak, (see Figure S1 in the Supporting Information), the XRD peaks of the Sample 2-7 shown in Figure 2a correspond with those of hexagonal hydroxyapatite (HAP) (JAPCS card # 09-0432). HAP is a mineral form from the apatite family, with a formula of $Ca_{10}(PO_4)_6(OH)_2$. The pK_{sp} (K_{sp} = solubility product) of HAP is 117.3 at 37 °C, which is significantly higher than other calcium phosphate phases (e.g., 6.6 for dicalcium phosphate dihydrate ($CaHPO_4{\cdot}2H_2O$) and 29.5 for β-tricalcium phosphate ($Ca_3(PO_4)_2$)). Therefore, HAP is regarded as the most stable phase of calcium phosphate within the pH range of 4.2-12.2.[25] Based on the result of ICP-MS, the proportion of P and Ca in the dried sample 2-7 was 13.04 wt % and 26.20 wt %, respectively, and thus the molar ratio P/Ca was calculated at 0.642, which is close to that of regular hydroxyapatite (i.e., P/Ca = 0.6). The ICP-MS result also evidenced the formation of hydroxyapatite.

Chemical bonding in the synthesized HAP@Alg nanoparticles was analyzed by FTIR spectra. As shown in Figure 2b and Figure S2 (Supporting Information), the bands at 1614 and 1416 cm^{-1} were the result of asymmetric (ν_8) and symmetric (ν_3) stretching vibrations of the C−O bond from the carboxylate group, respectively. The band at 2932 cm^{-1} is attributed to C−H stretching. In addition to the peaks corresponding to the organic alginate shell, the bands at 1096 and 1030 cm^{-1} can be attributed to the triply degenerate asymmetric stretching mode vibration (ν_3) of phosphate groups. The peak at 961 cm^{-1} is the non-degenerate symmetric stretching (ν_1) of phosphate groups. The peaks at 602 and 562 cm^{-1} result from the doubly degenerate bending mode (ν_4) of the P−O bond, and the peak at 472 nm^{-1} corresponds to the doubly degenerate bending mode (ν_2) of the same group. The FTIR spectra show the existence of both the inorganic HAP and the organic alginate component in the sample, which is consistent with the XRD and TEM results.

The thermogram of the HAP@Alg nanoparticles contrasts that of the pure alginate polymer. As shown in Figure 2c, three regions can be defined in the thermogravimetric analysis (TGA) curve for alginate. Initially, the weight loss was slow from 50 °C to 220 °C, which results from the desorption of weakly-bound water and lactonization.[26] It has been reported that commercial alginate contains moisture of up to 10 wt %.[27] In the region of 220−280 °C, the weight dropped dramatically, and this weight loss can be attributed to the decarboxylate of

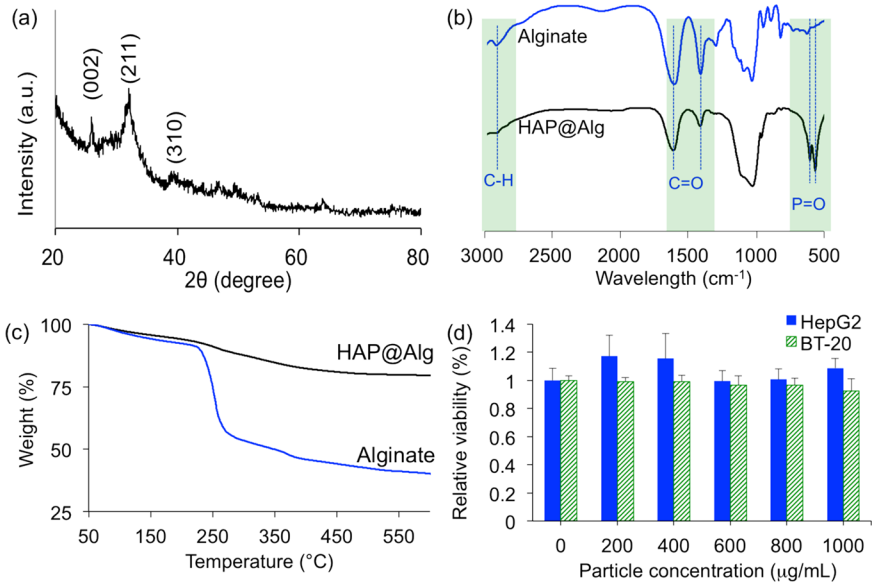

Figure 2. (a) XRD pattern of the synthesized HAP@Alg nanoparticles, (b) FT-IR spectra and (c) TGA profiles of alginate polymer and the synthesized HAP@Alg nanoparticles, and (d) cell viability of HepG2 and BT-20 cancer cells incubated with HAP@Alg nanoparticles for 24 h by MTT assays.

the alginate, in the form of CO_2, because COO^- groups usually decompose in this temperature range. In the third region of 280−600 °C, the gradual weight loss can be attributed to the loss of abundant hydroxyl groups in alginate.[28] In contrast to that of alginate, the TGA curve of HAP@Alg was smooth throughout the temperature range, remaining at a residual weight of 77.6 wt % after 600 °C. The weight loss in this case can be ascribed to the decomposition of the organic alginate shell. Therefore, estimating the residual weights of alginate and HAP@Alg, the proportion of alginate in the HAP@Alg nanoparticles was calculated at approximately 37.4 wt %. For comparison, we also performed the TGA curve of pure HAP nanoparticles (see Figure S3 in the Supporting Information), and it is clearly seen that there was no apparent weight loss during calcination.

3.2. Biocompatibility of HAP@Alg Nanoparticles. Safety is of utmost importance when nanoparticles are used for biomedical applications. Although both alginate and hydroxyapatite have been reported to exhibit high biocompatibility, the cytotoxicity of the newly synthesized materials in this study must be specified. MTT assay was used to quantify the effect of HAP@Alg nanoparticles on human breast cancer cells BT-20 and liver cancer cells HepG2. As shown in Figure 2d, our HAP@Alg clearly exhibited excellent biocompatibility, and no adverse effects were observed up to a high concentration of 1000 μg/mL. The excellent biocompatibility of HAP@Alg ensures its potential for use in biomedical applications such as drug delivery systems.

To visualize the intracellular uptake of our HAP@Alg nanoparticles, we tagged the samples with a cell membrane impermeable organic dye 5(6)-carboxyfluorescein (CF). This allowed us to observe the location of the internalized HAP@Alg nanoparticles through the fluorescent CF indicator. The HepG2 cancer cells were treated with CF-labeled HAP@Alg nanoparticles (size = 188.2 nm, PDI = 0.162, determined from DLS) and observed through a confocal laser scanning microscope. Cells were stained with a blue fluorescent dye (DAPI) to specify the location of the nuclei under UV radiation (Figure 3a). The CF-labeled HAP@Alg nanoparticles emitted green fluorescence under an excitation wavelength of 488 nm,

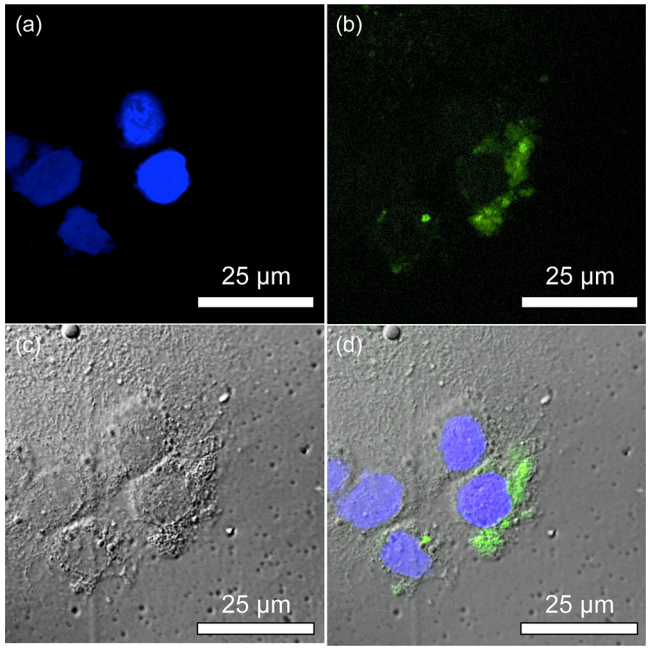

Figure 3. Confocal laser scanning microscope images of HepG2 cells treated with CF-labeled HAP@Alg nanoparticles for 2 h. (a) Nuclei are stained with DAPI. (b) Green dots indicate the location of CF-labeled HAP@Alg nanoparticles. (c) Cell morphologies are accessed by transmitted DIC microscope. (d) Merged images.

(Figure 3b). Cell morphologies were depicted in the DIC image (Figure 3c). Because CF is not permeable to cells themselves, the green fluorescence could only derive from the CF-labeled nanoparticles, indicating that the CF-labeled HAP@Alg nanoparticles were indeed uptaken by HepG2 cells and localized in the cytoplasm. The morphologies of the HepG2 cells did not change after endocytosis of the nanoparticles

(Figure 3d), thereby suggesting little or negligible cytotoxicity of our samples. This observation is in accordance with the results of the MTT assays. It is interesting to note that although we estimated the particle size to be around 100 nm by both direct SEM observation and DLS analysis, after HAP@Alg NPs were uptaken by cells, they aggregated inside the cells (in the cytoplasm) due to ionic interactions between charged HAP@Alg and cell medium. Therefore, only aggregated HAP@Alg NPs could be observed by confocal microscopy.

3.3. In vitro Loading and pH-Responsible Release of Drugs. To demonstrate the co-synthesis of drug-loaded HAP@Alg nanoparticles, we chose R6G, a positively charged, water-soluble dye, as the model drug because it can act as a surrogate for the most commonly used anti-cancer drug doxorubicin, with which it shares a similar molecular weight and charge. We used two in situ loading routes: first, R6G was dissolved in either alginate solution (route 1) or $CaCl_2$ solution (route 2), as shown in Scheme 1. Route 1 has been introduced in several other studies;[23,29] however, we expected route 2 to produce a higher loading efficiency, based on the formation mechanism of the HAP@Alg core−shell structure. All loading processes were conducted according to the synthetic conditions of sample 2-7.

For the loading of R6G through route 1, the loading amount increased with the increase in input amount of R6G from 0.5 to 2 mg and reached a plateau after 2 mg, as shown in Figure 4a.

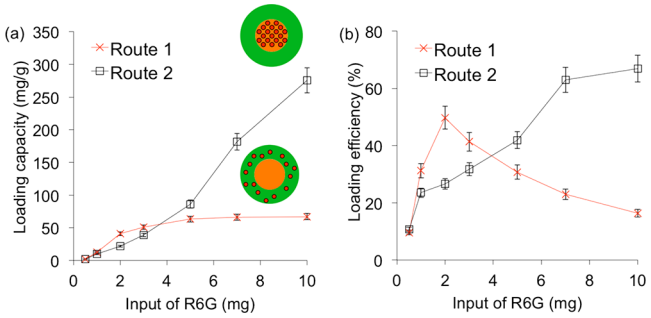

Figure 4. (a) Encapsulation capacity and (b) efficiencies of R6G into HAP@Alg nanoparticles through two different routes.

The loading efficiency also increased as the input of R6G increased from 0.5 to 2 mg, but then decreased when more R6G molecules were added (Figure 4b). We calculated the drug loading capacity to be approximately 65 mg for one gram of HAP@Alg nanoparticles, with a maximum efficiency of 50%. The low loading capacity of route 1 can be explained by the shelter effect of R6G. Because positively charged R6G molecules were added to the alginate solution before the addition of calcium, R6G molecules could interact with negatively charged alginate electrostatically. Although sequential additions of calcium and phosphate led to the formation of HAP@Alg nanoparticles, we suggest that most of the R6G molecules were still encapsulated in the alginate shell, and not in the HAP core, resulting in a low loading capacity, as shown in Scheme 1a.

For route 2, R6G molecules were mixed with Ca^{2+} solution. As shown in Figure 4, both the loading capacity and efficiency increased as the R6G input increased. The trend is very different from that of route 1, suggesting the presence of a different encapsulation mechanism. We propose that the positively charged R6G molecules helped Ca^{2+} interact with alginate; therefore they should be encapsulated within the HAP core during the formation of nanoparticles, as shown in Scheme 1b. Because of the limited solubility of R6G in the $CaCl_2$ solution (i.e., 7 mg of R6G in 5 mL of 0.04 M $CaCl_2$), the maximum loading amount was limited to 275 mg/g, with a high loading efficiency of 67%. These in situ loading strategies provide varying loading capacities, efficiencies, and locations for guest molecules in HAP@Alg nanoparticles, which influence the corresponding release behavior.

The release behavior of the loaded R6G molecules at varying pH values was also investigated. The release profiles of the R6G molecules encapsulated through the two routes are shown in Figure 5. For the R6G molecules encapsulated through route 1,

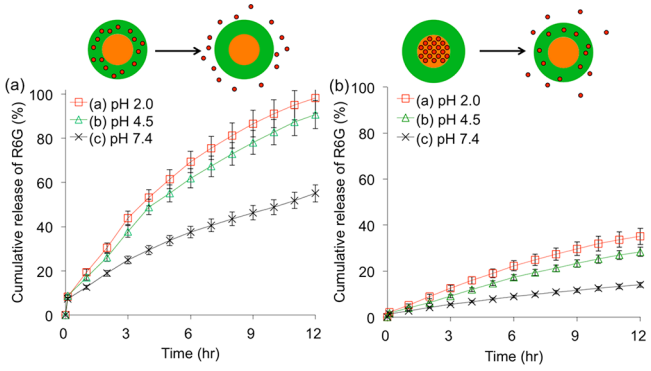

Figure 5. Cumulative release of R6G from HAP@Alg nanoparticles (synthetic condition 2−7, input R6G: 7 mg) prepared by (a) route 1 and (b) route 2. The release was conducted in 10 mM acetate buffers at different pH values and the temperature was kept at 37 °C.

the release rates were significantly higher at acidic conditions (pH 2.0 and pH 4.5) than at the physiologic condition (pH 7.4) (Figure 5a). For example, after 8 h, the release amounts of R6G at pH 2.0 and pH 4.5 were found to be 1.87- and 1.68-fold, respectively, the amount at pH 7.4. A similar pH-responsive controlled release behavior was observed for route 2 (Figure 5b). We propose that the pH-responsible release property is attributed to the higher solubility of HAP in acidic conditions. As shown in the Supporting Information, the release amount of R6G was found to be proportional to the release time for all cases, which indicates that the release kinetics were closed to the first-order release, rather than to the pseudo-first-order release that has been widely reported when drugs are loaded into porous nanocarriers.[30,31] This first-order release behavior suggests that the R6G was released upon the dissolution of the HAP core.

This hypothesis was confirmed by FTIR spectra of HAP@Alg nanoparticles after release at pH 2. As shown in Figure 6, for both route 1 and 2, the P−O−P bands disappeared after release, indicating a complete dissolution of HAP. In addition to the dissolution of the HAP core, the protonation/deprotonation of alginate at different pH values is also critical to the release behavior of guest molecules.[8] At low pH values, the carboxylate groups of alginate were protonated, so the electrostatic interaction between negatively charged alginate and positively charged R6G was diminished, resulting in higher release amounts. Another evidence was the TEM image of R6G-loaded HAP@Alg nanoparticles that were immersed at pH 2 for 12 h (see Figure S1 in the Supporting Information). From the TEM image, it is clearly seen that the HAP@Alg NPs

dx.doi.org/10.1021/am301895u | ACS Appl. Mater. Interfaces 2012, 4, 6720−6727

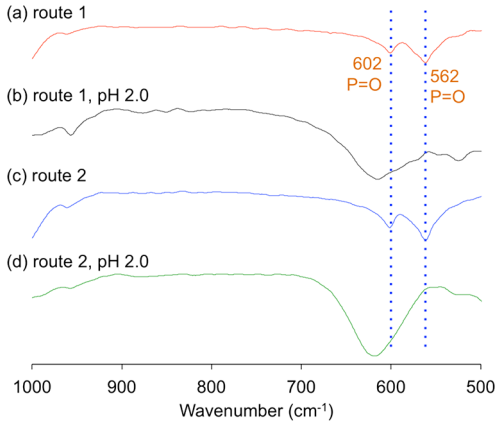

Figure 6. FTIR spectra of R6G-loaded HAP@Alg nanoparticles (prepared by route 1 and route 2) before and after release at pH 2.

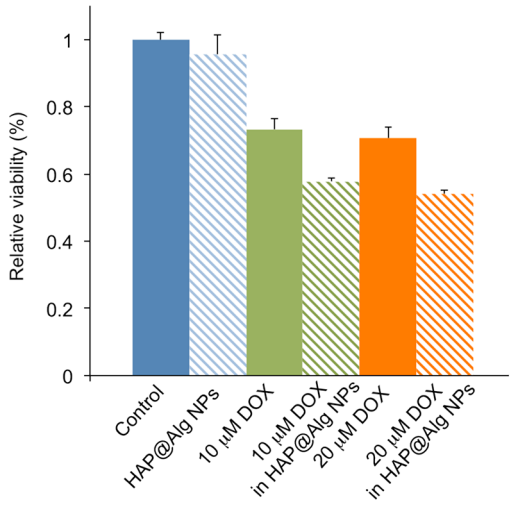

Figure 7. MTT assays of HepG2 cells treated with free DOX molecules and DOX-loaded HAP@Alg nanoparticles at various concentrations.

are uniform in size and the HAP cores were indeed dissolved in acidic conditions, which promote the release of R6G cargo.

Although route 1 and 2 exhibited similar pH-sensitive release behaviors, their release amount was different from each other. R6G molecules were loaded mostly in the alginate shell for route 1 and in the HAP core for route 2. Therefore, when the R6G-loaded HAP@Alg nanoparticles prepared for route 1 started to release, a burst release of 7% occurred at the initial stage. As the release time increased, HAP dissolved in the solutions and thus forced the diffusion of R6G from the alginate shell to its surroundings. As shown in Figure 5a, because of the lower loading amount in this case, most of the R6G molecules could be released (especially in acidic conditions) so the release efficiency was higher than the one in route 2. In contrast, when the R6G-loaded HAP@Alg nanoparticles prepared for route 2 started to release, no burst release occurred in the initial stage, and the total release efficiency was low (only 35%). In this case, the positively charged R6G molecules needed to diffuse from the HAP core (Figure 5b). In this case, most of R6G molecules were entrapped in the HAP core. We here demonstrate that different loading methods could selectively place guest molecules in the core or shell positions, which resulted in different release properties.

3.4. Intracellular Drug Delivery with Drug-Loaded HAP@Alg Nanoparticles. To investigate intracellular drug delivery by HAP@Alg, we chose a chemotherapeutic drug (i.e., doxorubicin (DOX)) and load it through route 2. The cell viability of BT-20 cells was evaluated by MTT assay after 16 h with different dosages of DOX-loaded HAP@Alg nanoparticles. The amount of DOX released from HAP@Alg was fixed at 10 and 20 M. For comparison, BT-20 cells were also treated with free DOX molecules at the same concentrations. As shown in Figure 7, the free DOX molecules exhibited weak cytotoxicity toward BT-20 cells (i.e., 73% viability for 10 μM). In contrast, the viability of cells treated with DOX-loaded HAP@Alg decreased to 58% under the same condition. This result suggests that the enhanced intracellular drug delivery was attributed to DOX-loaded HAP@Alg-mediated endocytosis. The suitable particle size (around 100 nm) of the HAP@Alg NPs and the biocompatible alginate shell enhanced cellular internalization, whereas the HAP core allowed drug loading. In addition, the acid-assisted biodegradability of the HAP core facilitated drug release in acidic endosomes or lysosomes after endocytosis. When HAP dissolves in acidic environments such as endosomes or lysosomes, the release of calcium and phosphate ions causes an osmotic pressure across the endosome membrane, which interrupts the endosome membrane and promotes the cargo to escape from the endosome to the cytoplasm, resulting in cell death.

4. CONCLUSION

This study reports the synthesis of hydroxyapatite/alginate (HAP@Alg) core−shell nanoparticles with controllable particle sizes through a pre-gel method. The synthesized HAP@Alg nanoparticles exhibit excellent biocompatibility, superior drug loading capacity, and enhanced drug release efficacy. Several guest molecules, such as organic dyes and therapeutic anticancer drugs, can be loaded efficiently into the core or shell position of the synthesized HAP@Alg, and released through acid-assisted dissolution controlled kinetics. The HAP@Alg nanoparticles show significant potential as effective and visually observable transmembrane delivery carriers for the intracellular controlled release of cell-membrane-impermeable drugs. Further development of this type of HAP@Alg material can lead to a new generation of nanodevices for biomedical applications.

■ ASSOCIATED CONTENT

Ⓢ Supporting Information

XRD pattern for a pure alginate polymer, FT-IR spectrum and TGA curve of a pure HAP nanoparticles, TEM image of a hollow alginate nanoparticle, and release kinetics of R6G-loaded HAP@Alg NPs (route 2). This material is available free of charge via the Internet at http://pubs.acs.org/.

■ AUTHOR INFORMATION

Corresponding Author

*E-mail: kevinwu@ntu.edu.tw.

Notes

The authors declare no competing financial interest.

■ ACKNOWLEDGMENTS

This research was supported by the National Science Council of Taiwan (100-2113-M-002-017, 101-2623-E-002-005-ET, and 101-2923-E-002-012-MY3) and by National Taiwan University Hospital (UN101-015).

REFERENCES

(1) Slowing, I. I.; Vivero-Escoto, J. L.; Wu, C.-W.; Lin, V. S. Y. *Adv. Drug Delivery Rev.* **2008**, *60*, 1278−1288.
(2) Ariga, K.; Lvov, Y. M.; Kawakami, K.; Ji, Q.; Hill, J. P. *Adv. Drug Delivery Rev.* **2011**, *63*, 762−771.
(3) Kawakami, K.; Ebara, M.; Izawa, H.; Sanchez-Ballester, N. M.; Hill, J. P.; Ariga, K. *Curr. Med. Chem.* **2012**, *19*, 2388−2398.
(4) Petros, R. A.; DeSimone, J. M. *Nat. Rev. Drug Discovery* **2010**, *9*, 615−627.
(5) Rejman, J.; Oberle, V.; Zuhorn, I. S.; Hoekstra, D. *Biochem. J.* **2004**, *377*, 159−169.
(6) Fadeel, B.; Garcia-Bennett, A. E. *Adv. Drug Delivery Rev.* **2010**, *62*, 362−374.
(7) George, M.; Abraham, T. E. *J. Controlled Release* **2006**, *114*, 1−14.
(8) Tonnesen, H. H.; Karlsen, J. *Drug Dev. Ind. Pharm.* **2002**, *28*, 621−630.
(9) Rajesh, P.; Khuller, G. Alginate as a Drug Delivery Carrier. In *Handbook of Carbohydrate Engineering*; CRC Press: Boca Raton, FL, 2005; pp 799−816.
(10) Ribeiro, C. C.; Barrias, C. C.; Barbosa, M. A. *Biomaterials* **2004**, *25*, 4363−4373.
(11) Zhu, H. G.; Srivastava, R.; Brown, J. Q.; McShane, M. J. *Bioconjugate Chem.* **2005**, *16*, 1451−1458.
(12) Joshi, A.; Keerthiprasad, R.; Jayant, R. D.; Srivastava, R. *Carbohydr. Polym.* **2010**, *81*, 790−798.
(13) de Lima, F. O.; Nonato, F. R.; Couto, R. D.; Barbosa Filho, J. M.; Nunes, X. P.; Ribeiro dos Santos, R.; Soares, M. B. P.; Villarreal, C. F. *J. Nat. Prod.* **2011**, *74*, 596−602.
(14) Lu, F.; Wu, S. H.; Hung, Y.; Mou, C. Y. *Small* **2009**, *5*, 1408−1413.
(15) Fernandez-Fernandez, A.; Manchanda, R.; McGoron, A. J. *Appl. Biochem. Biotechnol.* **2011**, *165*, 1628−1651.
(16) Mackiewicz, N.; Gravel, E.; Garofalakis, A.; Ogier, J.; John, J.; Dupont, D. M.; Gombert, K.; Tavitian, B.; Doris, E.; Duconge, F. *Small* **2011**, *7*, 2786−2792.
(17) Yu, H. J.; Zou, Y. L.; Wang, Y. G.; Huang, X. N.; Huang, G.; Sumer, B. D.; Boothman, D. A.; Gao, J. M. *ACS Nano* **2011**, *5*, 9246−9255.
(18) Chang, Y. L.; Meng, X. L.; Zhao, Y. L.; Li, K.; Zhao, B.; Zhu, M.; Li, Y. P.; Chen, X. S.; Wang, J. Y. *J. Colloid Interface Sci.* **2011**, *363*, 403−409.
(19) Chen, D. Y.; Li, N. J.; Xia, X. W.; Xu, Q. F.; Ge, J. F.; Li, Y. G.; Lu, J. M.; Gu, H. W. *J. Controlled Release* **2011**, *152*, E67−E68.
(20) Rajaonarivony, M.; Vauthier, C.; Couarraze, G.; Puisieux, F.; Couvreur, P. *J. Pharm. Sci.* **1993**, *82*, 912−917.
(21) Aleman, J.; Chadwick, A. V.; He, J.; Hess, M.; Horie, K.; Jones, R. G.; Kratochvil, P.; Meisel, I.; Mita, I.; Moad, G.; Penczek, S.; Stepto, R. F. T. *Pure Appl. Chem.* **2007**, *79*, 1801−1827.
(22) De, S. J.; Robinson, D. *J. Controlled Release* **2003**, *89*, 101−112.
(23) Yu, C.-Y.; Jia, L.-H.; Yin, B.-C.; Zhang, X.-Z.; Cheng, S.-X.; Zhuo, R.-X. *J. Phys. Chem. C* **2008**, *112*, 16774−16778.
(24) Murata, Y.; Nakada, K.; Miyamoto, E.; Kawashima, S.; Seo, S.-H. *J. Controlled Release* **1993**, *23*, 21−26.
(25) Uskokovic, V.; Uskokovic, D. P. *J. Biomed. Mater. Res., Part B* **2011**, *96B*, 152−191.
(26) Achelhi, K.; Masse, S.; Laurent, G.; Saoiabi, A.; Laghzizil, A.; Coradin, T. *Dalton Trans.* **2010**, *39*, 10644−10651.
(27) Zohuriaan, M. J.; Shokrolahi, F. *Polym. Test.* **2004**, *23*, 575−579.
(28) Tripathy, T.; Singh, R. P. *J. Appl. Polym. Sci.* **2001**, *81*, 3296−3308.
(29) Sarmento, B.; Ferreira, D.; Veiga, F.; Ribeiro, A. *Carbohydr. Polym.* **2006**, *66*, 1−7.
(30) Lian, H.-Y.; Liang, Y.-H.; Yamauchi, Y.; Wu, K. C. W. *J. Phys. Chem. C* **2011**, *115*, 6581−6590.
(31) Wu, K. C.; Yamauchi, Y.; Hong, C. Y.; Yang, Y. H.; Liang, Y. H.; Funatsu, T.; Tsunoda, M. *Chem. Commun.* **2011**, *47*, 5232−5234.